HHS Public Access

Author manuscript

Inorg Chem Commun. Author manuscript; available in PMC 2021 October 01.

Published in final edited form as:

Inorg Chem Commun. 2020 October ; 120: . doi:10.1016/j.inoche.2020.108154.

A New bis(rhodamine)-Based Colorimetric Chemosensor for Cu^{2+}

Fasil Abebe[*], **Jazmin Gonzalez**, **Khalil Makins-Dennis**, **Roosevelt Shaw**

Department of Chemistry, Morgan State University, Baltimore, MD, 21251

Abstract

A novel sensor (RD) bearing rhodamine B and 4-tert-Butyl phenol unit have been designed and synthesized using microwave irradiation. The sensor allows selective detection of Cu^{2+} by forming absorptive complex and trigger the formation of highly colored ring-open spirolactam. The recognition ability of the sensor was investigated by absorbance, Job's plot, infrared (IR) and time dependent-density functional theory (TD-DFT) calculations.

Keywords

Rhodamine; Sensor; Microwave; Absorbance; Colorimetric; Cu^{2+}

Introduction

Metals are inorganic molecules that are abundant in the human body and important for many metabolic processes. Transition and heavy metals enter the environment through industrial processes such as pharmaceutical production, agricultural pesticides, and corrosion of pipes. Being the third most prevalent metal in the body, copper plays a major role in oxygen transport, enzyme-catalyzed reactions, and electron transport [1]. In excess, copper can cause genetic mutations and neurological disorders such as Menkes syndrome, Wilson's disease and is linked to Alzheimer's disease [2]. Prolonged exposure to copper can also cause to liver and kidney damage leading to jaundice and hemolysis [3]. The World Health Organization (WHO) set the maximum concentration for copper in drinking water at 30μM and the acceptable daily consumption of copper should not exceed 12mg for adults [2]. To analyze drinking water supplies and monitor the intake of copper, the need for a selective and sensitive chemosensor is significant.

Optical chemosensors have become an important and widely used tool for real-time monitoring of metal ion concentration in biological samples. Most such sensors reported have a metal binding site linked to a fluorophore, and the metal binding causes the change in

[*]Authors to whom correspondence should be addressed; Fasil.Abebe@morgan.edu.

Declaration of competing interest

The authors declare that they have no known competing financial interests or personal relationships that could have appeared to influence the work reported in this paper.

absorbance and fluorescence intensity [4]. Selective detection of these metal ions has potential applications in many fields including: Chemistry, Medicine, Biology and Environmental sciences, therefore, there is a greater importance of developing selective chemosensors for biological metal ions.

Optical and colorimetric detection of metal ions is important as it is quite simple over the other detection techniques such as atomic absorption spectroscopy (AAS), Inductively coupled plasma mass spectrometry (ICP-MS) and cyclic voltammetry (CV) [5, 6]. Compared with traditional analytical methods, colorimetric methods can be achieved by ultraviolet visible (UV-Vis) absorption spectra with advantages such as easy operation and recognition, which can be used for on-site tests [7]. Rhodamine B derivatives have received a great deal of attention as chemosensors with useful properties such as: good solubility, low cytotoxicity, photostability, high absorption coefficient, and high fluorescent quantum yield [7,8]. Moreover, rhodamine B derivatives can undergo equilibrium between their spirocyclic and ring-open forms, which have completely different optical properties [10–14]. This phenomenon gives them an excellent potential for the development of turn-on optical sensors. Here we report new rhodamine-derived colorimetric sensor, which is rapid and selective, and capable of detecting paramagnetic Cu^{2+} in aqueous media. In this work, we introduce a microwave-assisted method to synthesize **RD** in a simple approach; the strategy is shown in scheme 1.

2. Experimental

2.1 Reagents

Unless otherwise statement, all chemical reagents and solvents were of analytical grade. Rhodamine B, hydrazine monohydrate and 4-tert-Butyl-2, 6-diformylphenol were purchased from Aldrich, and used without further purification. The stock solutions of metal ions were prepared from their nitrate and chloride salts. Distilled deionized water was used throughout the experiments. All the spectroscopic studies were performed in aqueous acetonitrile solution in which the sensors formed a colorless solution that was stable for more than a week.

2.2. Materials and instruments

Microwave-assisted organic synthesis reactions were carried out in a CEM microwave reactor. ^{1}H-NMR and ^{13}C-NMR spectra were recorded using an Avance 400 MHz NMR spectrometer (Bruker Biospin, Billerica, MA, USA). High resolution mass spectrometry (HRMS) were recorded using Bruker 12T solarix FT-ICR-MS. The IR spectrum was obtained using Shimad zu IRAffinity-1S FTIR spectrometer (Shimadzu Scientific, Columbia, MD, USA). All UV/Vis spectroscopy experiments were recorded using Agilent Cary 60 UV-Vis spectrometer (Agilent, Walnut Creek, CA, USA). Fluorescence emission experiments were measured using Varian Cary Eclipse fluorescence spectrophotometer (Varian, Walnut Creek, CA, USA), with excitation and emission slit widths of 5 nm and excitation wavelength at 510 nm.

2.3. Computational methods

Time dependent density functional theory (TD-DFT) calculations were employed to elucidate the Cu^{2+} interactions with **RD** system. All computations were carried out using Spartan'16 software package. Geometry optimization of the ground state structures was carried out with DFT at the B3LYP/6–31G (d) level of theory.

2.4. Microwave-assisted synthesis of compound RD

The intermediate compound **1** were synthesized according to the reported procedure [9]. A mixture of **1** (100 mg, 0.219 mmol), 4-tert-Butyl-2, 6-diformylphenol (22mg, 0.109 mmol), and ethanol (2 mL) was placed in a 10 mL reaction vial. The resulting mixture was stirred to make it homogeneous and it was placed in the cavity of a CEM microwave reactor. The closed reaction vessel was run under pressure and irradiated at a temperature of 100°C for 30 minutes. After cooling to room temperature, the resulting solid was filtered and washed three times with cold ethanol. After drying, the ligand **RD** was isolated to give in 83% yield. ^{1}H-NMR (DMSO), δ (ppm): 11.00 (1H, s, OH), 9.3 (2H, s, N=C-H), 7.97 (2H, m); 7.67 (5H, m), 7.40 (1H, s), 7.20 (2H, s), 6.40 (12H, m, H-Ar), 3.31 (16H, q, J=7.0 Hz, NCH_2CH_3), 1.15 (3H, s), 1.14 (6H, s), 1.13 (24H, t, J=7.0 Hz, NCH_2CH_3). ^{13}C-NMR (DMSO), δ (ppm): 163.10, 154.04, 153.06, 152.96, 149.93 (N=C-H), 148.72, 148.49, 148.40, 147.89, 141.47, 133.91, 132.72, 129.56, 129.05, 129.02, 127.98, 127.64, 127.07, 124.05, 123.15, 123.03, 119.95, 108.09, 107.96, 105.29, 104.96, 97.24, 97.15, 65.91 (spiro carbon), 43.64 (NCH_2CH_3), 33.81, 33.64, 30.75, 12.40, (NCH_2CH_3). Anal. Calcd for $C_{68}H_{74}N_8O_5$: H, 6.88; C, 75.39; N, 10.34. Found: H, 6.81; C, 75.31; N, 10.36. HRMS (MALDI): m/z Calcd for $C_{68}H_{74}N_8O_5$: 1083.5854; Found: 1083.5878.

3. Results and discussion

3.1 Selectivity of the colorimetric sensor for Cu^{2+}

The method of absorptivity and colorimetry plays an imperative role in the detection of copper ions. To investigate the selectivity of the sensor for the detection of Cu^{2+} over other interference ions (Na^+, K^+, Mg^{2+}, Ca^{2+}, Ni^{2+}, Zn^{2+}, Co^{2+}, Hg^{2+}, Pb^{2+}, Fe^{2+}, Fe^{3+}, and Cr^{3+}), the absorbance of **RD** in the separate presence of Cu^{2+} was determined, as well as in the presence of other possible interference ions individually. As shown in Fig. 1a, the absorbance of sensor **RD** significantly increased in the presence of Cu^{2+}, while the absorbance did not show obvious changes and difference from the blank in the presence of other metal ions. The results suggested that the sensor had an excellent selectivity towards Cu^{2+} over other interference ions. Because of the colorimetric method, we were able to clearly distinguish the sensing of Cu^{2+} ion using a sensor from other cations in the vicinity of naked eye color changes. The color of the solution changes from colorless "off" to pink red color "on", allowing "naked-eye" detection. Scheme 2 exhibits the naked-eye colorimetric change of **RD** with Cu^{2+}.

3.2 Sensing ability of RD

The metal ion sensing of **RD** was investigated by UV/Visible absorption spectra. The colorless solution showed no absorption above 450 nm, properties which are characteristic

of the predominant ring-closed spirolactam. The predominant spirolactam form was further confirmed by observation of the characteristic carbon resonance near 65.91 ppm. The UV/Vis spectrum of sensor recorded in buffer at 25°C and showed an absorption maximum at λ=312–320 nm, which is attributed to the intramolecular π-π* charge transfer transition (Fig 1b and S1b). Upon addition of Cu^{2+}, the main absorption peak at 320 nm decreased gradually, and a new absorption band appeared at 565 nm dramatically with the isosbestic point at 362 nm, which can be ascribed to the delocalized xanthene moiety of rhodamine (Fig. 1b). As shown in Fig. 1b, we observed gradual increases of this new peak up to 2.1 equiv. of Cu^{2+} ions. The detection limit of **RD** for Cu^{2+} ion was estimated based on the absorbance titration experiment as 0.26 μM. The complex association constant (K) calculated through Benesi-Hildebrand equation for Cu^{2+} with **RD** was found to be 4.4×10^8 M^{-2}. The colorimetric strategy toward Cu^{2+} was compared with some reported colorimetric methods for detection of Cu^{2+}, as listed in Table 1[20–29]. Our newly developed colorimetric and absorptive strategy presents a few attractive features, such as a high sensitivity, selectivity, short analysis time. This unique UV absorption change was not accompanied by the enhancement of fluorescence, which can be attributed to the inherent quenching property of paramagnetic Cu^{2+} [15,16]. When Cr^{3+} was added into the colorless solution of **RD**, fluorescent enhancement with an emission peak at 583 nm was observed. This demonstrate that **RD** is a specific turn-on fluorescent sensor for Cr^{3+}. The fluorescence responses of **RD** to different metal ions are shown in Fig. S1.

3.3 Binding mechanism of RD to Cu^{2+}

As the selectivity of the sensor has been confirmed, to further understand the recognition nature of **RD** to Cu^{2+} ions, we investigated the coordination mode between them. The stoichiometry for the binding between **RD** and Cu^{2+} was studied by Job's plot experiment. Sensor **RD** coordinated to Cu^{2+} with 1:2 stoichiometry in CH_3CN/H_2O (7:3 v/v) solution (Fig. 2a). Dimeric system **RD** containing phenol group can make 1:2 complex as shown in Scheme 2, which was reversible process. It is assumed that the spirolactam form was opened upon the addition of Cu^{2+} to sensor and make a highly delocalized π-conjugated stable complex with Cu^{2+} through their active donor sites of receptor part, though other ions failed which basically indicates that the coordinate moiety of **RD** matches perfectly with Cu^{2+} ions instead of the other metal ions. To confirm the mechanism of interaction between sensor and Cu^{2+}, IR analysis was also conducted besides the Jobs plots analysis. From this spectral analysis, it has been observed that the characteristic starching frequency of the carbonyl of **RD** appears at 1724 cm^{-1}. This peak is completely disappeared in IR spectrum of Cu^{2+} complex. Similarly, the imine (-CH=N-) frequency shifted from 1617 cm^{-1} to 1589 cm^{-1} and the hydroxyl (-OH) stretching band broadened after complexation with Cu^{2+} ion (Fig. 2b and Fig. S6). A sharp peak at 1315 cm^{-1} indicates the presence of the nitrate group in the complex. ^1H NMR was also performed by adding Cu^{2+} to the DMSO-d_6 solution of **RD** as shown in Fig. 3. The **Rd**-Cu^{2+} complex was prepared by the additions of 0.5 and 1.0 equivalent $Cu(NO_3)_2$ to the DMSO solution of **RD**. The peaks observed at δ 11 and δ 9.5 are attributable to the phenolic OH and the imine proton (-CH=N-) in **RD,** respectively. Various aromatic protons appear in the range of 6–9 ppm. Addition of 0.5 and 1 equiv. of Cu^{2+} resulted in the disappearance and slight down filled of the hydroxyl proton indicating the binding of Cu^{2+} ion through the phenoxide interaction. The partial ^1H NMR spectrum of **RD**

shows the signal at δ 9.5 corresponds to imine hydrogen which gets shifted down filled with the addition of Cu^{2+} ions. These results indicate that carbonyl O, imine N and phenoxide oxygen are surely involved in Cu^{2+} coordination.

3.4 Reversibility of RD

Cyanide ions known to coordinate with Cu^{2+} ions to form a very stable complex Cu $(CN)_x$ [16–18], we have investigated selectivity of the RD-Cu^{2+} complex toward CN^- using the cooper-cyanide affinity. As demonstrated above, the absorbance intensity of **RD**-Cu^{2+} complex reached the maximum value when 2.1 eq. of Cu^{2+} were added. To evaluate the selectivity of the **RD**-Cu^{2+} complex toward various anions (CN^-, ClO_4^-, CH_3COO^-, HSO_4^-, $H_2SO_4^{2-}$, SCN^-, Cl^-, I^-, F^-, OH^-) in CH_3CN-H_2O solution, we conducted the absorption experiment by using UV/Vis spectroscopy. Figure S2 shows the addition of 20 μM of anions to **RD**-Cu^{2+} (1:2) of which CN^- alone decreases the absorption peak at 565 nm, indicating high selectivity for CN^-. The addition of CN^- to the **RD**-Cu^{2+} solution led to a change in color of the solutions from pink to colorless, which was observed with the naked eye. This result strongly supports **RD**-Cu^{2+} binds CN^- ions with higher selectivity and the process is reversible. The proposed binding mechanism of **RD** with Cu^{2+} in the presence and absence of CN^- shown in Scheme 2.

3.6 Computational studies of RD and its dimeric RD-Cu^{2+} complex

Time-Dependent Density Functional Theory (TD-DFT) calculations using Spartan ‘18 software was employed to elucidate the Cu^{+2} interactions with sensor **RD**. Both sensor **RD** and its dimeric **RD**-Cu^{+2} complex were optimized in the gas phase (vacuum) and in both simulated CH_3CN and simulated water media using the conductor-like polarizable continuum model (CPCM) at the (DFT) B3LYP/6–31G (d) level of theory. TD-DFT calculations were then used to compare the vertical electronic excitations of optimized structures with empirical obtained UV-vis data.

In vacuum, two prominent vertical excitations are computed for **RD**, one at 335.64 nm with f = 0.4488 and a second one at 369.00 nm with f = 0.1462. The energy gap between the highest occupied molecular orbital (HOMO = −4.81 eV) and the lowest unoccupied molecular orbital (LUMO= −1.32 eV) for **RD** is 3.49 eV (λ = 355.26 nm). For dimeric **RD**-Cu^{+2} complex in vacuum, the prominent vertical excitation is at 573.87 nm (f = 0.0028). The frontier energy gap for this complex in vacuum is 2.82 eV (HOMO = −10.78 eV, LUMO = −7.96 eV) (Fig. 4). In CH_3CN, two prominent vertical excitations are present as well for **RD**, one at 321.61 nm with f = 0.8803 and the second one at slightly longer wavelength, 369.72 nm (f = 0.7151). The frontier energy gap is 3.17 eV (HOMO = −5.02 eV, LUMO = −1.85 eV). For dimeric **RD**-Cu^{+2} complex in CH_3CN, two prominent vertical transitions appear, both with equal f values (f = 0.0052) and wavelengths of 574.75 nm and 575.17 nm. The frontier energy gap for this complex in CH_3CN is 2.77 eV (HOMO = −5.62 eV, LUMO = −2.85 eV) (Fig. S7 and S8). In water, two prominent transitions again occur for **RD**, one at 318.59 nm (f=0.8923) and the second one also at longer wavelength, 365.88 nm (f = 0.5841). As in CH_3CN, the frontier energy gap is also 3.17 eV (HOMO = −5.03 eV, LUMO = −1.86 eV). For dimeric **RD**-Cu^{+2} complex in water, the prominent vertical transition

occurs at 568.71 nm (f=0.0038). The frontier energy gap for this complex in water is 2.79 eV (HOMO = −5.55 eV, LUMO = −2.76 eV) (Fig. 5).

In the three media above, both the HOMO and LUMO of **RD** appear to be unchanged in their locations. The HOMO is found primarily on one of the two xanthene moieties while the LUMO is delocalized over the two spirolactam moieties, the two imine groups, and the connecting phenolic ring. In these same media, the HOMO of **RD**-Cu^{+2} complex appears to be unchanged in its location and is found primarily on one of the two xanthene moieties; however, in vacuum the LUMO of **RD**-Cu^{+2} complex is delocalized over the center part of the complex, extending outward from phenoxide ring but not found over the phenoxy oxygen and appearing faintly over the Cu^{+2} ions. In both CH_3CN and water, the LUMO of **RD**-Cu^{+2} complex is found over the opposite xanthene moiety.

Conclusion

In summary, we synthesized a new bis(rhodamine)-based colorimetric and absorptive sensor for Cu^{2+}. This spirolactam compound showed excellent selectivity for Cu^{2+} in CH_3CN/H_2O tris-HCl buffer over other common cations. The colorimetric and absorbance response to Cu^{2+} can be conveniently detected even by the naked eye, which provides a facile method for visual detection of Cu^{2+}.

Supplementary Material

Refer to Web version on PubMed Central for supplementary material.

Acknowledgements

This work was supported by the National Institute of General Medical Sciences of the National Institutes of Health under Award Number SC2GM125512 and Morgan State University.

Reference

1. Jiang R; Liu N; Li F; Fu W; Zhou Y; Zhang Y Novel PSMA-coated on-off-on fluorescent chemosensor based on organic dots with AIEgens for detection of copper (II), Iron (III) and cysteine. Polymers. 10, 2018, 786.
2. Liu S; Wang Y-M; Han J Fluorescent chemosensors for copper (II) ion: Structure, mechanism and application. Journal of Photochemistry and Photobiology C: Photochemistry Reviews. 32, 2017, 78–103.
3. Yuan L; Lin W; Chen B; Xie Y Development of FRET-based ratiometric fluorescent Cu^{2+} chemodosimeters and the applications for living cell imaging. Organic Letters. 14, 2012, 432–435. [PubMed: 22201292]
4. Asiri A; Sobahi T; Mohammad Al-Amari M; Asad M; Zayed M; Khan S Physicochemical investigation of HDDP azomethine dye as turn-on fluorescent chemosensor for high selectivity and sensitivity of Al^{3+} ions. Journal of Solution Chemistry. 47, 2018, 1711–1724.
5. Li C; Xiang K; Liu Y; Zheng Y; Tian B; Zhang J A novel colorimetric chemosensor for Cu^{2+} with high selectivity and sensitivity based on Rhodamine B. Research on Chemical Intermediates. 41, 2015, 10169–10180.
6. Wang Y; Song F; Zhu J; Zhang Y; Du L; Ka C Highly selective fluorescent probe based on a rhodamine B and furan-2-carbonyl chloride conjugate for detection of Fe^{3+} in cells Tetrahedron Letters. 59, 2018, 3756–3762.

7. Wan J; Zhang K; Li C; Li Y; Niu S A novel fluorescent chemosensor based on a rhodamine 6G derivative for the detection of Pb^{2+} ion. Sensors and Actuators B: Chemical, 246, 2017, 696–702.
8. Du W; Cheng Y; Shu W; Wu B; Kong Z; Qi Z The influences of different substituents on spectral properties of rhodamine B based chemosensors for mercury ion and application in EC109 cells. Canadian Journal of Chemistry. 95, 2017, 751–757.
9. Leite A, Silva A, Cunha-Silvs L, Castro B, Gameiro P, Rangel M Discrimination of fluorescence light-up effects induced by PH and metal ion chelation on a spirocyclic derivative of rhodamine B. Dalton Transactions. 42, 2013, 6110–6118 [PubMed: 23299402]
10. Gao Z; Kan C; Liu H; Zhu J; Bao X A highly sensitive and selective fluorescent probe for Fe^{3+} containing two rhodamine B and thiocarbonyl moieties and its application to live cell imaging. Tetrahedron, 75, 2019, 1223–1230.
11. Weerasinghe A, Oyeamalu A, Abebe F; Venter A; Sinn E Rhodamine based turn-on sensors for Ni^{2+} and Cr^{3+} in organic media: detecting CN− via the metal displacement approach. Journal of Fluorescence, 26(3), 2016, 891–898. [PubMed: 26994908]
12. Abebe F; Sutton T; Perkins P; Makins-Dennis K; Winstead A Microwave-assisted synthesis of rhodamine derivatives. Green Chemistry Letters and Reviews, 11:3, 2018, 237–245. [PubMed: 32194653]
13. Formica M; Fusi V; Giorgi L; Micheloni M New fluorescent chemosensors for metal ions in solution. Coordination Chemistry Reviews. 256, 2012, 170–192.
14. Abebe F; Sutton T; Perkins P; Shaw R Two colorimetric fluorescent turn-on chemosensors for detection of $Al^{3+}$and N3−: Synthesis, photophysical and computational studies. Luminescence. 33, 2018, 1194–1201. [PubMed: 30091286]
15. DeSilva A; Gunaratne H; Gunnlaugsson T; Huxley T; McCoy C; Rademacher J; Rice T Signaling recognition events with fluorescent sensors and switches. Chemical Reviews. 97, 1997, 1515–1566. [PubMed: 11851458]
16. Cheng D; Liu X; Yang H; Zhang T; Han A; Zang L A Cu2+-selective probe based on phenanthrol-imidazole derivative. Sensors. 17, 2017, 35, 1–8.
17. Jung HS; Han JH; Kim ZH; Kang C; Kim JS Coumarin-Cu(II) Ensemble-Based Cyanide Sensing Chemodosimeter. Org. Lett 13, 2011, 5056–5059. [PubMed: 21875122]
18. Liu Y; Lv X; Zhao Y; Liu J; Sun Y-Q; Wang P; Guo W A Cu(ii)-based chemosensing ensemble bearing rhodamine B fluorophore for fluorescence turn-on detection of cyanide. J. Mater. Chem 22, 2012, 1747–1750.
19. Bhalla V; Singh H; Kumar M Triphenylene based copper ensemble for the detection of cyanide ions. Dalton Trans. 41, 2012, 11413–11418. [PubMed: 22890983]
20. Peng J; Liu G; Yuan D; Feng S; Zhou T A flow-batch manipulated Ag NPs based SPR sensor for colorimetric detection of copper ions in water samples. Talanta. 167, 2017, 310–316. [PubMed: 28340726]
21. Yin K; Li B; Wang X; Zhang W; Chen L Ultrasensitive colorimetric detection of Cu2+ ion based on catalytic oxidation of L-cysteine. Biosens Bioelectron. 64, 2015, 81–87. [PubMed: 25194800]
22. Gao Q; Ji L; Wang Q; Yin K; Li J; Chen L Colorimetric sensor for highly sensitive and selective detection of copper ion. Analytical Methods. 9, 2017, 5094–5100.
23. Hanmeng O; Chailek N; Charoenpanich A; Phuekvilai P; Sanmanee N; Sirirak J; Swanglap P; Wanichacheva N Cu^{2+}-selective NIR fluorescence sensor based on heptamethine cyanine in aqueous media and its application. Spectrochimica Acta Part A. 2020, 118606.
24. Durai W; Ramu A Hydrazone based dual-responsive colorimetric and ratiometric chemosensor for the detection of Cu2+/F- ions: DNA tracking, practical performance in environmental samples and toothpaste. Journal of Fluorescence. 30, 2020, 275–289. [PubMed: 31997143]
25. Gunnlaugsson T; Leonard J; Murray N Highly selective colorimetric naked-eye Cu(II) detection using an azobenzene chemosensor. 6, 2004, 1557–1560.
26. Joo D; Mok J; Bae G; Oh S; Kang J; Kim C Colorimtric detection of Cu2+ and fluorescent detection of PO43- and S2- by a multifunctional chemosensor. 56, 2017, 8399–8407.
27. Patra V; Boricha V; Paul P Dual -mode calixarene-based chemosensor: highly selective fluorogenic detection of Hg^{2+} and chromogenic detection of Cu^{2+} with a single ionophore. Eur. J. Inorg. Chem 2019, 2019, 199–205.

28. Gupta V; Mergu N; Kumawat L A new multifunctional rhodamine-derived probe for colorimetric sensing of Cu(II) and Al(III) and fluorometric sensing of Fe(III) in aqueous media. Sensors and Actuators B Chem. 223, 2016, 101–113.

29. Guo S; Liu G; Fan C; Pu S A new diarylethene-derived probe for colorimetric sensing of Cu(II) and fluorometric sensing of Cu(II) and Zn(II): Photochromism and high selectivity. Sensors and Actuators B Chem. 266, 2018, 603–613.

Author Manuscript

Author Manuscript

Author Manuscript

Highlights

- An efficient, clean, and straightforward procedure to prepare rhodamine derivative using microwave-assisted organic synthesis
- The sensor showed fast absorbance response, excellent selectivity, and high sensitivity towards Cu^{2+}
- TD-DFT calculations supported the experimental data.

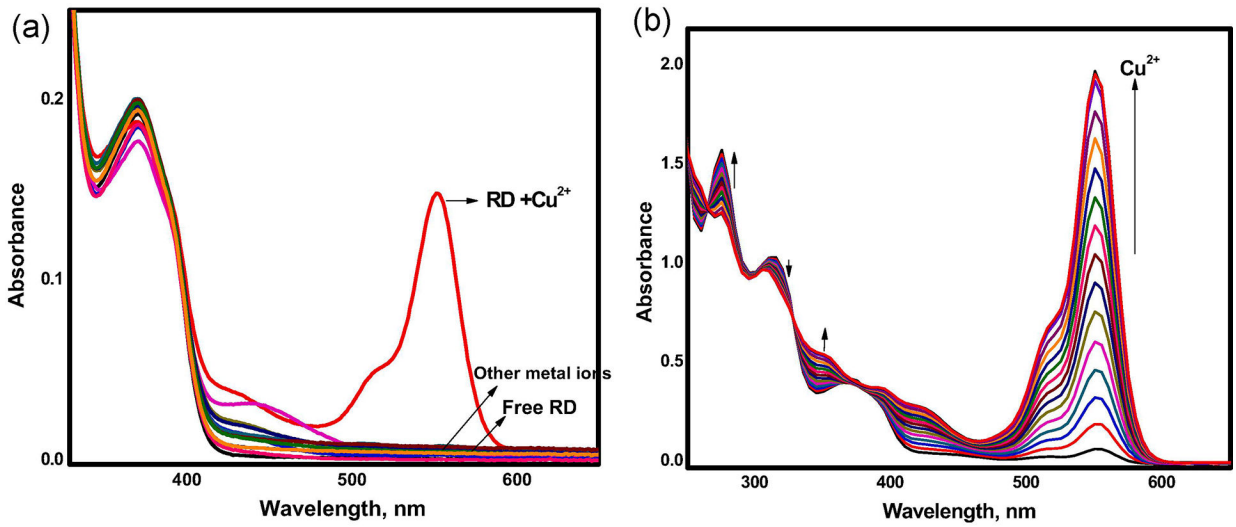

Fig. 1.

(a) UV-Vis spectra of **RD** (10μM) with metal ions in CH_3CN/H_2O (7:3 v/v) solution. (b) UV-Vis spectra of **RD** (10μM) with Cu^{2+} (0–20μM) in CH_3CN/H_2O (7:3 v/v) solution.

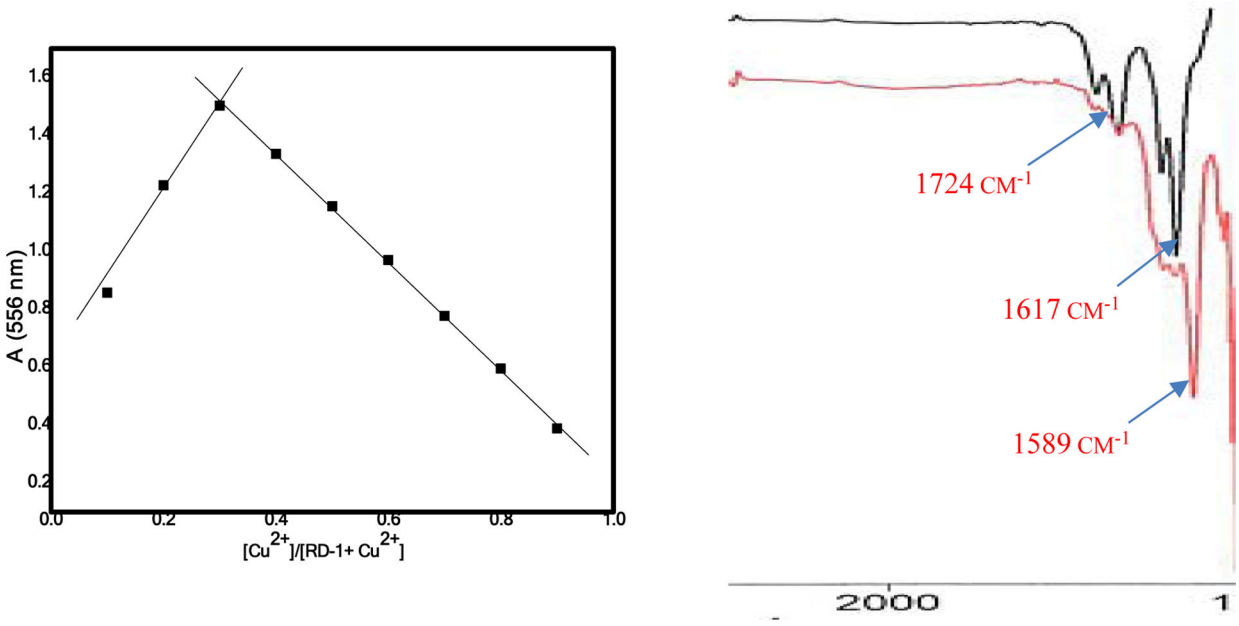

Fig.2.

(a) Jobs plot for compound **RD** with Cu^{2+} in CH_3CN-Tris-HCl (10 mM, pH =7.2) buffer. (b) IR spectra of **RD** and **RD**-Cu^{2+}

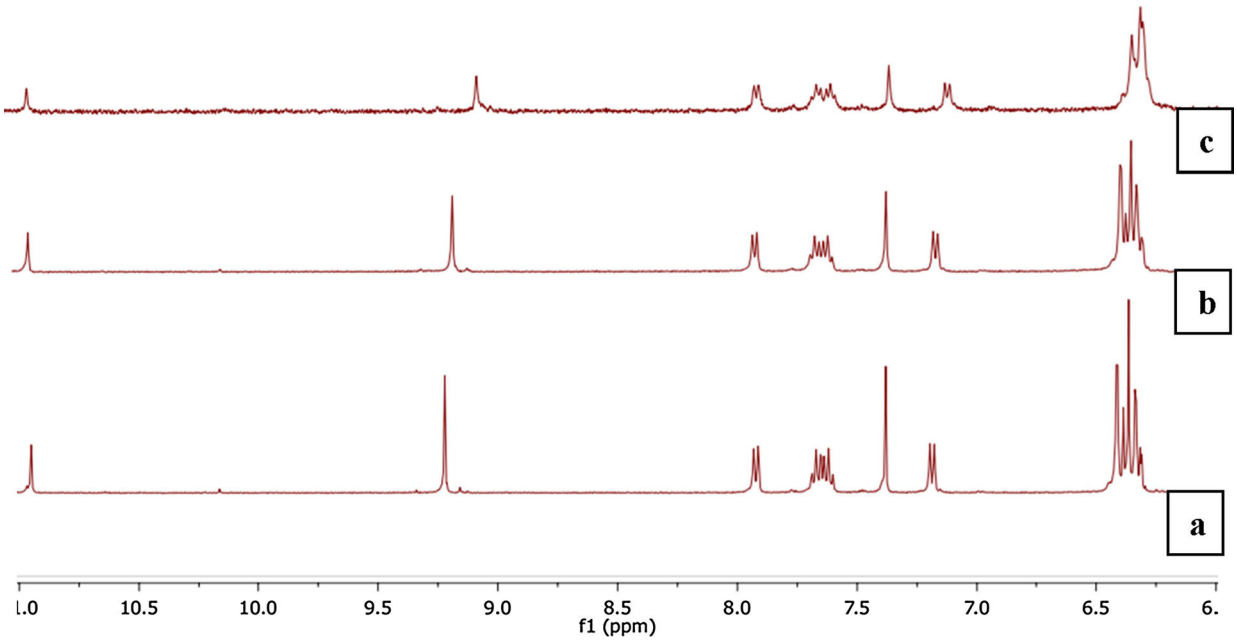

Fig. 3.

Partial ^{1}H NMR titration of **RD** with Cu^{2+} ions in DMSO-d_6. [(**a**) **RD** (**b**) **RD**: Cu^{2+} (0.5 equiv.) and (c) **RD**: Cu^{2+} (1 equiv.)

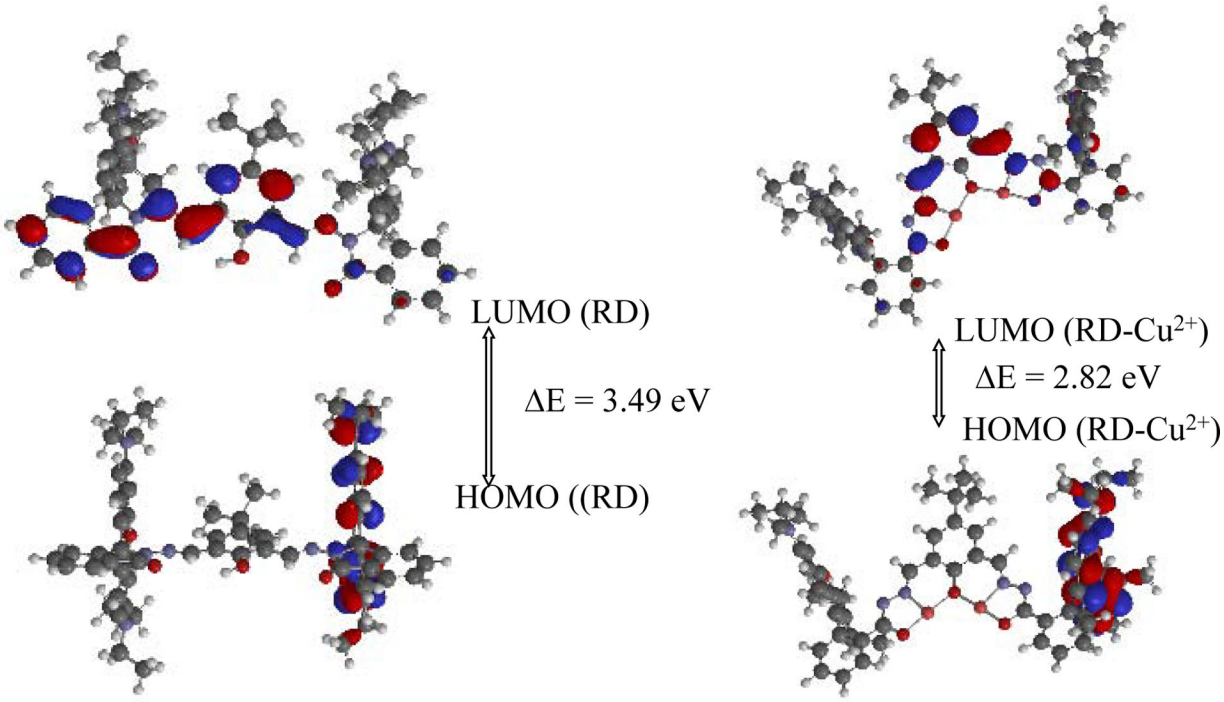

Fig. 4.

Electronic distribution of HOMO and LUMO energy levels of optimized **RD** and dimeric **RD**-Cu^{2+} complex in gas phase.

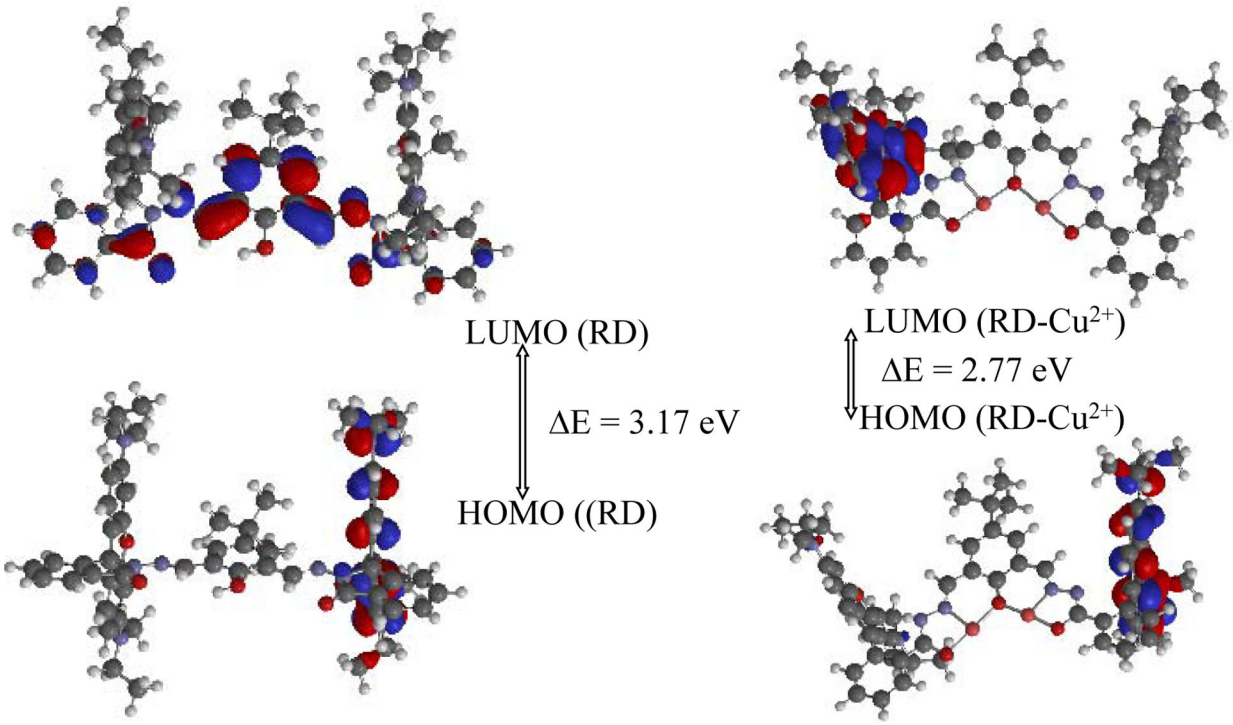

Fig. 5.

Electronic distribution of HOMO and LUMO energy levels of optimized **RD** and dimeric **RD**-Cu^{2+} complex in water.

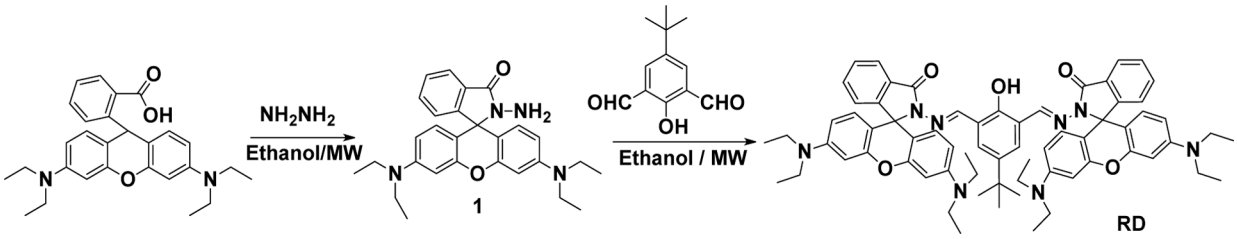

Scheme 1.
Microwave-assisted synthesis of **RD**

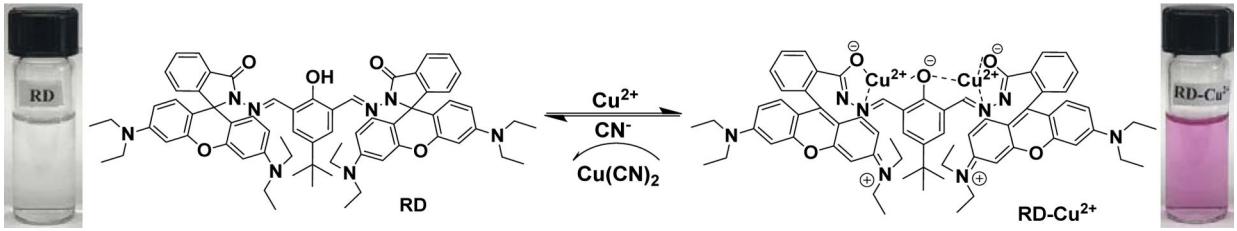

Scheme 2.

A possible proposed binding mechanism of sensor **RD** towards Cu^{2+} in the presence and absence of cyanide ion.

Table 1.

Comparisons of Cu^{2+} colorimetric sensors recently reported.

Sensing material	System	LOD	Real sample	Ref.
Ag NPs	Ammonium buffer	0.24 μg L^{-1}	Water samples	20 (2017)
L-cysteine	HEPES buffer	0.5 nM	Water and biological	21 (2015)
Cyanine-NB	PBS buffer	8.6 nM	Water sample	22 (2017)
Colorimetric	HEPES buffer:CH_3CN	4.7×10^{-8}		23 (2020)
Naphthalene	DMSO	5.8 μM	Water samples	24 (2020)
Azobenzene	HEPES	2 pM		25 (2004)
Phthalimide	Buffer: DMF (3;2 v/v)	5.8 μM	Water samples	26 (2017)
Calixarene	CH_3CN	2.5 μM		27 (2019)
Rhodamine	Aqueous	0.01 μM		28 (2016)
Diarylethene	CH_3OH	0.54 μM		29 (2018)
Rhodamine	CH_3CN:H_2O (7:3 v/v)	0.26 μM		This work